Discovery of Small-Molecule Inhibitors of the NFAT−Calcineurin Interaction by Competitive High-Throughput Fluorescence Polarization Screening[†]

Michael H. A. Roehrl,[‡,§] Julia Y. Wang,[||] and Gerhard Wagner*[,‡]

Department of Biological Chemistry and Molecular Pharmacology, Harvard Medical School, 240 Longwood Avenue, Channing Laboratory, Department of Medicine, Brigham and Women's Hospital, 181 Longwood Avenue, and Graduate Program in the Biological and Biomedical Sciences, Division of Medical Sciences, Faculty of Arts and Sciences, Harvard University, 220 Longwood Avenue, Boston, Massachusetts 02115

Received August 16, 2004; Revised Manuscript Received October 15, 2004

ABSTRACT: The direct protein−protein interaction between the phosphatase calcineurin and transcription factor NFAT plays important roles in a number of crucial mammalian cell signaling and regulatory events, such as activation of T cells and developmental genetic programs. In this paper, we report on the identification of small organic molecules for the targeted disruption of the NFAT−calcineurin interaction *in vitro*. In the preceding paper (*21*), we devise a theoretical and procedural framework for high-throughput fluorescence polarization screens to aid in this effort. The results presented here ground on this work and illustrate the stringency and successful general applicability of our approach. The identified compounds provide valuable molecular tools for probing calcineurin signaling and for the NFAT-specific inhibition of calcineurin in cells and organisms.

The targeted manipulation of protein−protein interactions by small molecules is rapidly gaining importance in the development of biological tools for dissecting living processes on a molecular level and for the discovery of conceptually novel drugs (*1*−*6*). A particularly interesting example, from a fundamental biological perspective and of great medical and therapeutic significance, is the interaction between the serine/threonine phosphatase calcineurin (Cn)[1] and the nuclear factor of activated T cells (NFAT) (*7*−*14*).

The calcium- and calmodulin-mediated dephosphorylation of NFAT by Cn triggers the nuclear translocation of transcription factor NFAT and initiates the transcription of crucial target genes involved in processes such as activation of the immune system or developmental genetic programs (*7*, *12*). Inappropriate activation of Cn is intimately linked to important states of disease, e.g., rejection of organ transplants, autoimmunity, or cardiac hypertrophy (*15*−*19*). Hence, it would be greatly significant to be able to specifically manipulate this signaling pathway.

The current strategic dogma for the pharmacological disruption of enzyme−substrate interactions is the complete inhibition of enzymatic activity. In the case of Cn, such is the mechanism of action of the powerful immunosuppressive drugs cyclosporin A and FK506 (*19*). However, multisubstrate enzymes such as Cn, which can act upon a diverse array of substrates besides NFAT (depending on cell type, intracellular localization, or signaling state), are shut down indiscriminately by this approach (*14*). Moreover, it is thought that many undesired or toxic side effects may arise from this nonselective strategy (*19*).

An entirely different line of attack is to directly target and disrupt the protein−protein interaction between the enzyme and a specific substrate, while leaving the catalytic functionality of the enzyme intact. The conceptual advantage of such a tactic is that other classes of substrates of the given enzyme could still be treated physiologically, since the inhibition would be substrate-specific. We have recently introduced this idea as substrate-selective enzyme inhibition (SSEI) (*20*).

Here, we provide a detailed quantitative analysis of the identification and validation of selective inhibitors of the NFAT−Cn interaction. This analysis employs our theoretical and procedural framework for protein−protein interaction assays based on fluorescence polarization (FP), which is described in the preceding paper (*21*). We apply our new concepts to the focused identification and characterization of small-molecule inhibitors of NFAT−Cn association (INCAs) *in vitro*, with both complete and incomplete dissociation capabilities. The compounds are promising tools for the study of cell signaling and can serve as lead scaffolds for the development of conceptually novel drugs.

ASSAY DEVELOPMENT

High-throughput (HTP) FP assays are typically designed to faithfully model protein−protein interactions *in vitro*. The initial steps of assay development are preparation and

[†] Support from the NIH (Grants GM038608 and AI037581 to G.W.) is gratefully acknowledged. Purchase and maintenance of equipment used for this research were supported by NIH Grants RR000995 and GM047467.

* To whom correspondence should be addressed: Department of Biological Chemistry and Molecular Pharmacology, Building C1, Harvard Medical School, 240 Longwood Ave., Boston, MA 02115. E-mail: gerhard_wagner@hms.harvard.edu. Phone: (617) 432-3213. Fax: (617) 432-4383.

[‡] Harvard Medical School.

[§] Harvard University.

[||] Brigham and Women's Hospital.

[1] Abbreviations: Cn, calcineurin; FP, fluorescence polarization; HTP, high-throughput; NFAT, nuclear factor of activated T cells; OG, Oregon Green.

10.1021/bi048232o CCC: $27.50
Published on Web 11/26/2004

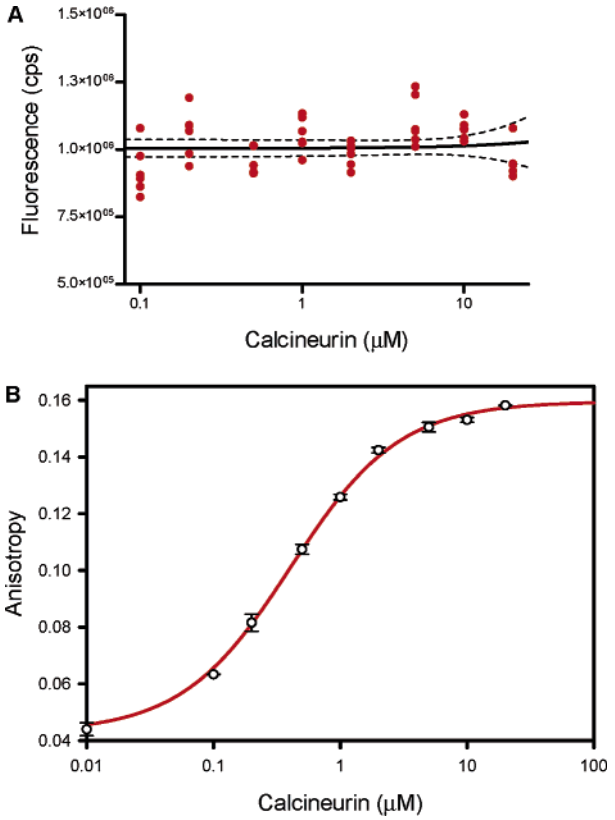

FIGURE 1: (A) Total fluorescence intensity of 30 nM OG-VIVIT as a function of Cn concentration (counts per second). Each dot denotes an individual, independent measurement. The fraction of bound OG-VIVIT ranges from 0% (0 μM Cn) to >97.5% (20 μM Cn). The solid and dashed lines denote the linear regression and its 95% confidence interval, respectively. Note that the abscissa is plotted logarithmically. The Cn concentration and fluorescence intensity are statistically not correlated ($P = 0.66$). (B) Direct binding experiment with 30 nM OG-VIVIT. Data fitting using eqs 6 and 39 from ref *21* yielded the red curve with the following parameters: $K_{D1} = 0.50 \pm 0.03$ μM, $A_B = 0.1596 \pm 0.0011$, and $A_F = 0.0429 \pm 0.0015$.

validation of the labeled probe. In the case of the NFAT−Cn interaction, we used the VIVIT peptide system as a surrogate for NFAT (*22*, *23*) and the recombinantly produced catalytic core of human Cn A, as previously described (*20*). Variables and equations not explicitly introduced in this paper are defined as they are in ref *21*. Our general strategy follows the procedures developed in ref *21*. It is generally optimal to use the fluorophore-labeled peptide at a concentration that is at least 1 order of magnitude below the K_D of the interaction. Here, we used a concentration of 30 nM.

As a basis for the analysis of FP data, one needs to investigate whether the association of Oregon Green (OG)-labeled VIVIT with Cn influences the detected total fluorescence intensity (quantum yield) of the fluorophore. This influence can generally be identified as Q, the I_B/I_F ratio of fluorescence intensities of bound (I_B) and free (I_F) labeled species measured under the same experimental conditions (*21*). We performed a direct binding experiment and devised a statistical approach to evaluating such potential bias (Figure 1A). Using 30 nM OG-VIVIT, we estimated I_F and I_B to be $(9.0 \pm 0.5) \times 10^6$ and $(9.6 \pm 0.7) \times 10^6$ cps, respectively. The Cn concentration (ranging from 0 to 20 μM) and fluorescence intensity were statistically uncorrelated ($P = 0.66$) with a Pearson correlation coefficient, r, of only 0.064 (Figure 1A) (*24*). Hence, we concluded that Q was not significantly different from unity and used a Q of 1 throughout our subsequent analysis. A rational approach to an estimate of Q is desirable, since biological systems have been described in which Q deviates significantly from unity, leading to potentially significant misinterpretation of FP data (*25*).

To determine the equilibrium dissociation constant K_{D1} for binding of the labeled peptide to Cn, we measured the fluorescence anisotropy as a function of total Cn concentration (Figure 1B). The experimentally observed anisotropies, A_{OBS}, were globally fitted to eqs 6 and 39 from ref *21*. We determined completely bound, A_B, and free, A_F, anisotropies of 0.1596 ± 0.0011 and 0.0429 ± 0.0015, respectively. For the dissociation constant K_{D1} between OG-VIVIT and Cn, we obtained a nonlinear least-squares estimate of 0.50 ± 0.03 μM.

A potential general problem for any binding and competition experiment is nonspecific interaction of binding partners. Therefore, we examined whether the anisotropies observed in the direct binding experiment were consistent with a specific direct binding model, or whether potential nonspecific binding effects would have to be attributed. In FP, the observed anisotropy, A, of a specific molecular species can be expressed as in eq 1 (*21*).

$$A = \left(1 + \frac{\tau_F}{\tau_C}\right)^{-1}\left(\frac{3\cos^2\kappa - 1}{5}\right)\left(\frac{3\cos^2\lambda - 1}{2}\right) = \left(1 + \frac{\tau_F}{\tau_C}\right)^{-1} \times A_0 \quad (1)$$

where τ_F is the fluorescence lifetime of the fluorophore (~4 ns for OG), τ_C denotes the rotational correlation time of the observed species, κ corresponds to the angle between absorption and emission transition dipoles, and λ represents the angle associated with the local motion of the fluorescent moiety. The product of the two trigonometric terms in eq 1 is known as the limiting anisotropy, A_0 (*21*). We define $\tau_C \equiv \tau_{CB}$ in the bound state and $\tau_C \equiv \tau_{CF}$ in the free state. The value of κ has been determined to be ~10.3° for fluorescein-based fluorophores such as OG (*26*). Using eq 37 from ref *21*, we estimated τ_{CB} of the bound OG-VIVIT−Cn complex to be approximately 16.3 ns ($M = 39\,631$ Da). Knowledge about A_B, τ_F, τ_{CB}, and κ allowed us to estimate λ as ~34.4°. We interpret this result as an indication that the OG label attached to VIVIT retains a certain degree of independent local mobility, a finding consistent with the functional observations that (i) fluorescence intensity was not influenced by VIVIT−Cn binding and (ii) the fluorophore did not affect competition with unlabeled VIVIT (*vide infra*). Similarly, τ_{CF} of free OG-VIVIT was estimated to be ~1.1 ns ($M = 1874$ Da) assuming an approximate prolate ellipsoid geometry (see section 1 of the Appendix). Using our estimates of τ_F, τ_{CF}, κ, and λ permitted an independent and quasi-*ab initio* calculation of A_F, yielding an A_F of 0.0434 via eq 1. The prediction is in excellent agreement with the experimentally measured value of A_F (0.0429 ± 0.0015, *vide supra*), indicating that the direct binding between OG-VIVIT and Cn was consistent with a purely specific model without significant nonspecific binding to Cn or other components of the system (*21*). Alternative approaches to such estimates are available but yield essentially similar results (*27*).

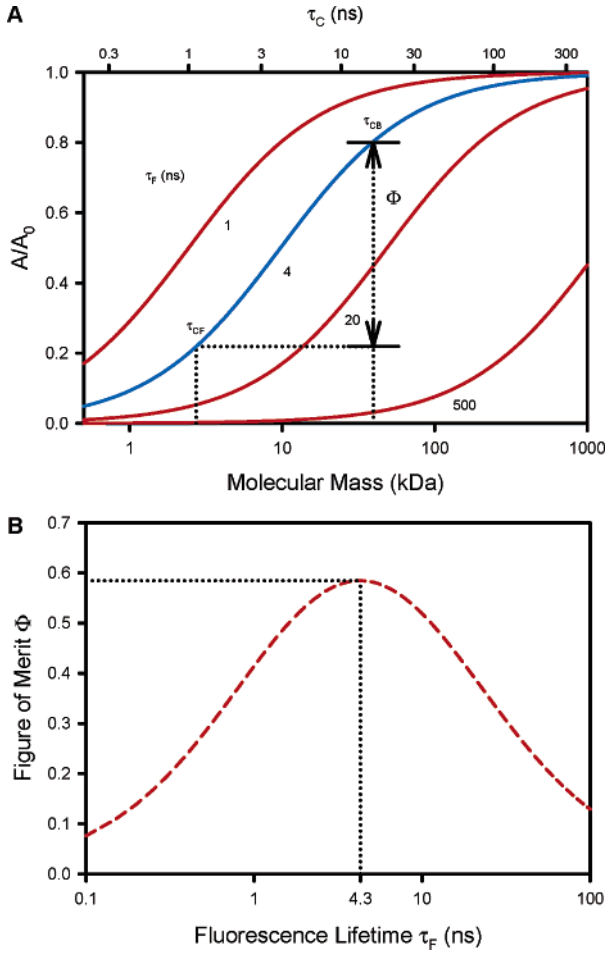

FIGURE 2: (A) Ratio of anisotropy, A, and limiting anisotropy, A_0, as a function of the approximate molecular mass of the labeled species and fluorescence lifetime, τ_F. The dotted lines and the blue curve indicate the situation for free OG-VIVIT and the OG-VIVIT−Cn complex, respectively. The figure of merit, Φ, is close to optimal under these conditions. The top abscissa indicates roughly corresponding rotational correlation times. Examples of fluorophores represented by the curves are fluorescein, rhodamine, and OG (all ~4 ns), AEDANS (20 ns), and ruthenium tris(2,2′-bipyridyl) (500 ns). (B) Figure of merit, Φ, as a function of fluorescence lifetime, τ_F, of the fluorophore for the interaction between OG-VIVIT and Cn. An optimum is reached when $\tau_F = 4.3$ ns (dotted lines).

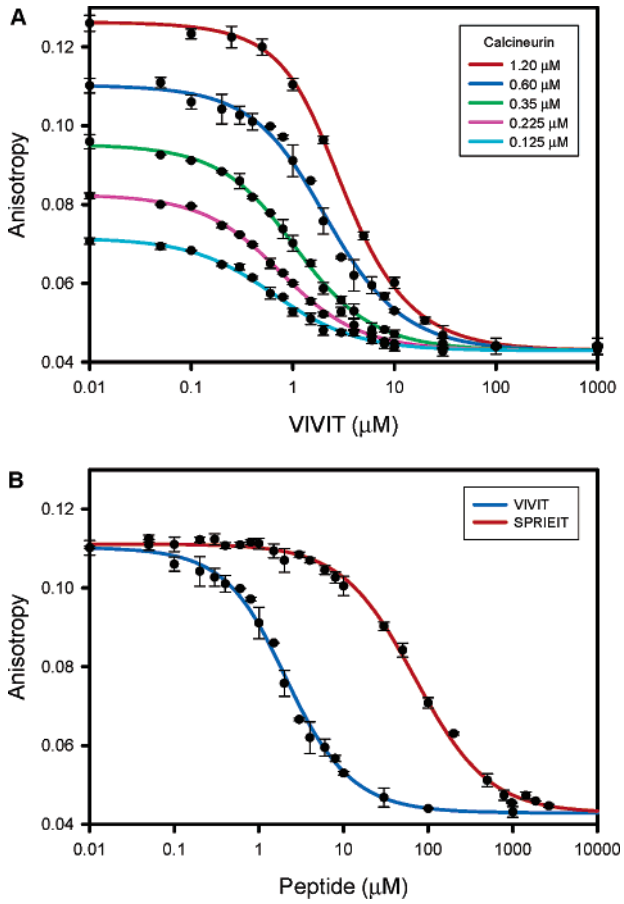

FIGURE 3: (A) Competitive displacement analysis of the OG-VIVIT−Cn complex by unlabeled VIVIT for various Cn concentrations (see the inset). Either 30 nM (red curve) or 60 nM (all others) OG-VIVIT was used. Nonlinear least-squares fitting yielded a K_{D2} of 0.48 ± 0.05 μM. At 0 μM on the abscissa (not shown because of the logarithmic scale), the respective ordinate value is defined as A_U (*21*). (B) Comparison of competitive displacement by VIVIT and SPRIEIT. The VIVIT curve (blue) is the same as in panel A and is shown for reference. Fitting the SPRIEIT curve (red) yielded a dissociation constant of 27.3 ± 1.4 μM. In both experiments, 0.60 μM Cn and 60 nM OG-VIVIT were used.

Knowledge about the molecular masses and, hence, appoximate rotational correlation times of free and bound species also allowed us to define the expected dynamic range of FP anisotropy (Figure 2A). For the specific regime of OG-VIVIT and Cn, a short fluorophore lifetime of ~4 ns is superior to both much shorter or longer lifetimes (see section 2 of the Appendix). In fact, the figure of merit, Φ, has a global optimum at $\tau_F = 4.3$ ns, which means that, under the given conditions, the chosen fluorophore was expected to provide nearly maximal discriminative power and sensitivity (Figure 2B). This approach to Φ is generally applicable and can be a guide in optimal fluorophore selection.

We next performed competitive binding assays using both labeled OG-VIVIT and unlabeled VIVIT (Figure 3A). Combining experimental data using five different Cn concentrations (0.125−1.2 μM) and globally fitting the data to eqs 17 and 39 from ref *21*, we determined dissociation constant K_{D2} for unlabeled VIVIT and Cn to be 0.48 ± 0.05 μM. This value is in excellent agreement with dissociation constant K_{D1} of OG-VIVIT (*vide supra*), corroborating that the fluorophore is functionally inert with respect to the interaction.

The sequence of the VIVIT peptide had originally been identified by combinatorial optimization of Cn binding affinity, starting from the corresponding wild-type sequence motif of NFAT (SPRIEIT peptide) (*22*, *23*). However, neither the affinity of the wild-type NFAT−Cn interaction nor the degree of optimization that had been achieved was quantitatively known. We tested the SPRIEIT peptide in the competitive assay and obtained a dissociation constant of 27.3 ± 1.4 μM (Figure 3B). Even though this value was obtained for an isolated peptide−protein interaction, one may expect that the physiologic dissociation constant of the NFAT−Cn interaction is similar in terms of the order of magnitude. This is because the SPRIEIT peptide by itself can dissociate the complete NFAT−Cn complex (*22*), indicating that overall binding contributions outside the SPRIEIT interface are comparatively small. The degree of affinity improvement from SPRIEIT to VIVIT is hence ~55-fold, corresponding to a decrease of the free energy of binding of approximately −9.8 kJ/mol. This improvement

Table 1: Optimal Fraction of Bound OG-VIVIT (F_{SB}) and Corresponding Optimal Cn Concentration for Various Projected Target Values of the Compound Dissociation Constant, K_{D2} (*21*)[a]

K_{D2} (μM)	∞	100	10	5	2.5	1	0.5	0.1	0.05	0.01
optimal F_{SB}	0.51	0.50	0.49	0.47	0.44	0.39	0.34	0.22	0.17	0.09
optimal [Cn] (μM)	0.53	0.52	0.49	0.45	0.41	0.33	0.27	0.15	0.11	0.05

[a] An OG-VIVIT concentration of 30 nM and a K_{D1} of 0.5 μM were assumed. For the HTP assay, a Cn concentration of 0.50 μM was chosen so that the assay had optimal discriminative power for the accurate estimation of dissociation constants with values of ≥10 μM (shaded columns). Compounds with dissociation constants with values of <10 μM would be identified as hits; however, the precision of estimating K_{D2} would not be optimal. For accurate follow-up titration experiments with high-affinity compounds, the Cn concentration was lowered accordingly.

Table 2: Signal-to-Noise Ratios (S/N) and Z' Factors Calculated for 30 nM OG-VIVIT and Cn Concentrations Ranging from 0.01 to 20 μM[a]

	0.01 μM Cn	0.10 μM Cn	0.20 μM Cn	0.50 μM Cn	1.0 μM Cn	2.0 μM Cn	5.0 μM Cn	10 μM Cn	20 μM Cn
S/N	0.2	5.2	5.9	13.0	19.2	23.1	22.1	26.2	29.1
Z'	<0	0.41	0.29	0.68	0.79	0.83	0.81	0.85	0.89

[a] The actual condition used in the HTP FP assay is shaded.

is particularly adventageous for HTP small-molecule screening, as described later.

During assay development, we established that (i) OG-VIVIT fluorescence intensity was not influenced by Cn binding, (ii) experimentally measured anisotropy values supported a purely specific binding behavior of OG-VIVIT, and (iii) dissociation constants of the labeled and unlabeled VIVIT peptide were virtually identical. The latter argument also implied that the interaction between unlabeled VIVIT and Cn was specific. Taken together, these findings set the stage for the subsequent high-throughput (HTP) competition assay for the identification of inhibitors of the VIVIT−Cn interaction.

HTP ASSAY

As shown in the preceding paper (*21*), HTP FP assays can be optimized for certain sets of *a priori* known or expected parameter values. Here, we desired to identify small-molecule inhibitors of the VIVIT−Cn interaction. The potency of a potential hit compound will depend on its specific dissociation constant for dissociation from Cn, K_{D2}. Using eqs 43 and 46 from ref *21*, we calculated the optimal initial fraction of bound OG-VIVIT and the corresponding optimal Cn concentration for various target values of K_{D2} (Table 1). The objective of a good HTP FP assay regime is to reliably separate low-affinity and/or nonspecific compounds on one hand from high-affinity, specific hit compounds on the other. We wanted to be able to distinguish dissociation constants with values of ≥10 μM optimally (shaded columns of Table 1). During initial screening, we deemed it less important to extract precise values for compounds with dissociation constants with values of <10 μM because such very active hits would, in any case, be later characterized individually in optimized titration experiments. Both goals could be accomplished by choosing a Cn concentration of 0.5 μM for the HTP assay.

A complementary approach to HTP assay design is the analysis of statistical quality parameters, such as the signal-to-noise ratio (S/N) and Z' factor (*28*). We determined both parameters for various concentrations of Cn and 30 nM OG-VIVIT (Table 2). Typically, an assay in which $0.5 \leq Z' \leq 1$ is considered excellent because of a large separation band and dynamic range. These findings together with the preceding optimization result corroborated the decision to use 0.50 μM Cn.

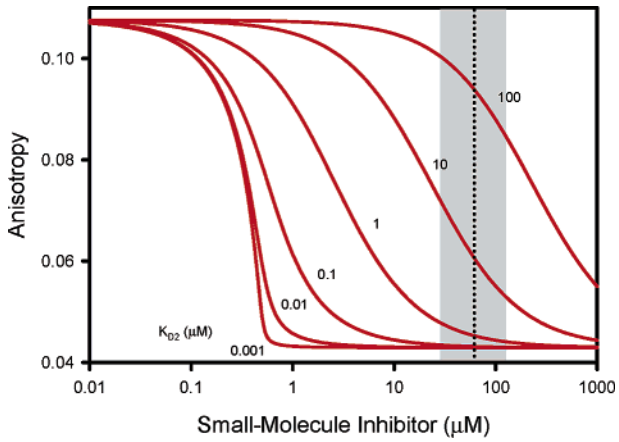

FIGURE 4: Predicted anisotropy values for competitive FP experiments with 0.5 μM Cn, 30 nM OG-VIVIT, and a K_{D1} of 0.5 μM. Curves for inhibitor−Cn dissociation constants (K_{D2}) ranging from 0.001 to 100 μM are plotted as functions of the small-molecule inhibitor concentration. Chemical libraries were screened at a constant mass per volume by adding 40 nL of 5 mg/mL stock solutions to 10 μL samples. This resulted in an effective concentration range of 28.5−126.7 μM (shaded area) with a median of 61.8 μM (dotted line).

At this point, it was possible to predict expected FP response curves as a function of both screening concentration and dissociation constant K_{D2} of a potential small-molecule inhibitor (Figure 4). Qualitatively, it can be seen that, at actually screened compound concentrations (shaded area in Figure 4), compounds with dissociation constants of approximately ≤1 μM would lead to the virtually complete reduction of anisotropy to the free baseline value, compounds with dissociation constants of ∼10 μM would show a significant reduction, and compounds with dissociation constants of approximately ≥100 μM would have a small or negligible influence on anisotropy. These results illustrate how we tuned assay parameters and screened compound concentrations to identify inhibitors for which $K_{D2} \leq 100$ μM.

Analogous calculations using the SPRIEIT peptide as a hypothetical probe revealed two major advantages of VIVIT affinity optimization (*22*, *23*) before embarking on an HTP FP assay: (i) A screen based on SPRIEIT would require ∼26.5 μM or 53 times more Cn to achieve similar signal-to-noise and Z' values. (ii) Compounds that were to be screened at effective concentrations near or below 26.5 μM

Table 3: Twenty Most Active Hit Compounds from the HTP FP Assay with 16 320 Compounds and Two Examples of Functionally Inactive Compounds (N-1 and N-2)[a]

rank	acronym	chemical formula	mass (Da)	Lipinski	R_1 (%)	R_2	R_3 (μM)	R_4 (%)
1	INCA-1	$C_{20}H_{13}ClO_6$	384.8	4	−99.3	−17.7	0.15	−2.9
2	INCA-2	$C_{16}H_9Cl_2NO_3S$	366.2	4	−95.6	−17.0	1.1	−8.0
3	INCA-3	$C_{14}H_{15}N_3O_2$	257.3	4	−95.4	−17.0	1.6	−8.7
4	−	$C_8N_{16}O_4$	384.2	3	−85.1	−15.2	3.9	+2.9
5	INCA-6	$C_{20}H_{12}O_2$	284.3	4	−83.0	−14.8	6.2	+2.9
6	INCA-5	$C_{16}H_{22}N_6O$	314.4	4	−80.7	−14.4	6.5	+4.0
7	INCA-7	$C_{11}H_{15}BrO_9$	371.1	4	−74.0	−13.2	8.1	−1.1
8	INCA-8	$C_{16}H_{17}BrClNO_3S_2$	450.8	3	−68.1	−12.1	8.9	+4.9
9	INCA-9	$C_{14}H_{17}Br_3N_2O_2$	485.0	4	−58.8	−10.5	12.4	+4.0
10	−	$C_{10}H_7BrCl_3NO_4$	391.4	4	−59.7	−10.6	14.8	+5.8
11	−	$C_{31}H_{16}N_2O_8$	544.5	2	−51.1	−9.1	15.1	+6.8
12	−	$C_{12}H_7N_3O_6$	289.2	4	−64.6	−11.5	16.3	−14.2
13	INCA-12	$C_{11}H_7NO_4$	217.2	4	−70.9	−12.6	16.3	−3.1
14	−	$C_{13}H_{13}ClN_2O_2S$	296.8	4	−63.8	−11.4	16.5	+8.8
15	−	$C_{14}H_{12}N_2O_4S$	304.3	4	−62.5	−11.1	17.0	−3.6
16	INCA-10	$C_{15}H_{13}N_3O_2S$	299.4	4	−62.5	−11.1	17.3	−14.4
17	INCA-19	$C_{11}H_{17}NO_3S$	243.3	4	−66.3	−11.8	18.0	−0.2
18	−	$C_8H_6N_6O_8$	314.2	3	−59.7	−10.6	18.6	−3.1
19	−	$C_{13}H_{12}N_2O_2S$	260.3	4	−62.1	−11.1	20.2	−4.5
20	−	$C_{14}H_{16}N_2O_2S$	276.4	4	−60.2	−10.7	20.7	+8.0
	N-1	$C_{15}H_{16}O_3$	244.3	4		not active		+0.6
	N-2	$C_{17}H_{13}BrN_2O_2$	357.2	4		not active		+3.6

[a] Hits were sorted by the R_3 ranking parameter. Ranking parameters were defined according to ref *21*. In brief, R_1 is a linearized change of anisotropy model, R_2 is a σ deviation model, R_3 is a single-point estimate of K_{D2}, and R_4 is a total fluorescence change control parameter. The Lipinski score can range from 0 to 4, with 4 denoting most druglike compounds (*29*).

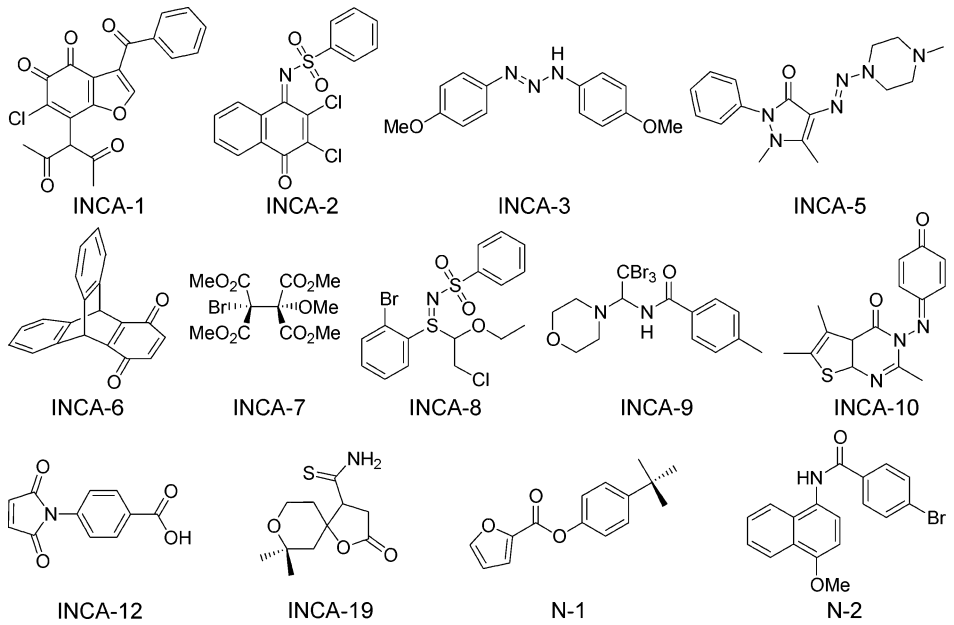

FIGURE 5: Chemical structures of selected INCA compounds that were characterized in detailed titration competition experiments. N-1 and N-2 are examples of inactive compounds.

(e.g., because of low aqueous solubility or higher molecular mass when used at a constant mass per volume) may be falsely identified as inactive (see also the leend of Figure 4). This false-negative effect would constitute a severe shortcoming of the assay, since it becomes more pronounced as the affinity of a potential hit increases. In contrast, the analogous threshold for VIVIT is ~0.5 μM and hence much below actual compound screening concentrations.

We subsequently screened 16 320 small molecules semi-robotically in the HTP FP assay for their ability to disrupt the VIVIT−Cn interaction, as described elsewhere in more detail (*20*). Ranking parameters R_1−R_4 were calculated for every measurement (*21*). Table 3 lists the 20 most active compounds sorted by their single-point predicted dissociation constants (R_3) together with two examples of inactive compounds. Since R_3 is based on a measurement at a single compound concentration, the parameter is associated with a considerable degree of uncertainty. This is why absolute values of R_3 can only be expected to correlate roughly with precise parameter estimates from detailed titration experiments. The chemical structures of compounds that were subsequently characterized in detailed competitive titration analyses (INCA compounds and inactive controls) are depicted in Figure 5. Hit compounds vary in mass from 217.2 to 544.5 Da and have mostly high, i.e., druglike, Lipinski scores of 3 or 4 (*29*). Inspection of the R_4 parameter indicated

Table 4: Quantitative Analysis of INCA Binding Affinities[a]

acronym	K_{D2} (μM)	K_{D3} (μM)
INCA-1	0.50 ± 0.09	–
INCA-2	0.12 ± 0.03	–
INCA-3	2.31 ± 0.59	7.71 ± 1.02
INCA-5	4.45 ± 0.55	11.77 ± 1.18
INCA-6	0.80 ± 0.11	–
INCA-7	0.32 ± 0.08	14.24 ± 2.35
INCA-8	2.33 ± 0.44	6.62 ± 0.59
INCA-9	11.88 ± 1.79	4.42 ± 0.29
INCA-10	4.09 ± 0.31	8.76 ± 0.46
INCA-12	0.44 ± 0.10	3.06 ± 0.14
INCA-19	29.52 ± 9.54	3.92 ± 0.70

[a] INCA-1, INCA-2, and INCA-6 completely displace VIVIT from Cn, whereas other INCAs have partial displacement capability.

no systematic influence of compound activity on emitted fluorescence intensity (*21*).

FOLLOW-UP TITRATION EXPERIMENTS WITH HIT COMPOUNDS

In analogy to experiments with VIVIT and SPRIEIT (Figure 3), detailed competitive FP titrations were carried out with each INCA compound and with N-1 and N-2. As expected, the negative control compounds N-1 and N-2 did not affect anisotropy and hence the OG-VIVIT−Cn complex up to concentrations of at least 1 mM. All 11 tested INCA compounds were found to be active upon detailed reexamination and reduced anisotropy significantly in a dose-dependent manner. The absence of false positives indicates high specificity and stringency of assay conditions and data ranking. This more quantitative follow-up analysis integrates many data points for each compound and, therefore, yields more accurate dissociation constant estimates than the initial crude single-point HTP ranking estimates (compare Tables 3 and 4).

INCA compounds fell into two classes, i.e., compounds that were able to dissociate the OG-VIVIT−Cn complex completely (INCA-1, INCA-2, and INCA-6), and compounds that afforded significant but partial dissociation (other INCAs, Figure 6). Some biophysical and functional aspects of the first class have been described elsewhere (*20*). The behavior of the second class is intriguing. One explanation could be that the compounds had reached their solubility limits. However, this was not true for at least the majority of our compounds (*20*). Further possibilities may include incomplete covalent modification or interference with VIVIT or the fluorophore. However, we did not detect any significant changes in fluorescence intensity in the presence of INCA compounds. An alternative model, which can explain the experimental findings, is the simple extension of a three-state competitive model to a four-state anticooperative model (*21*).

In the four-state model, a ternary inhibitor−OG-VIVIT−Cn complex is introduced as an additional permitted state. The model is described by three independent dissociation constants, of which K_{D1} and K_{D2} have identical significance as in the three-state model. K_{D3} describes the dissociation of OG-VIVIT from the ternary complex and allows for mutual ligand affinity modulation.

We have previously shown that if $K_{D3} > K_{D1}$, the model predicts that OG-VIVIT will dissociate more readily from

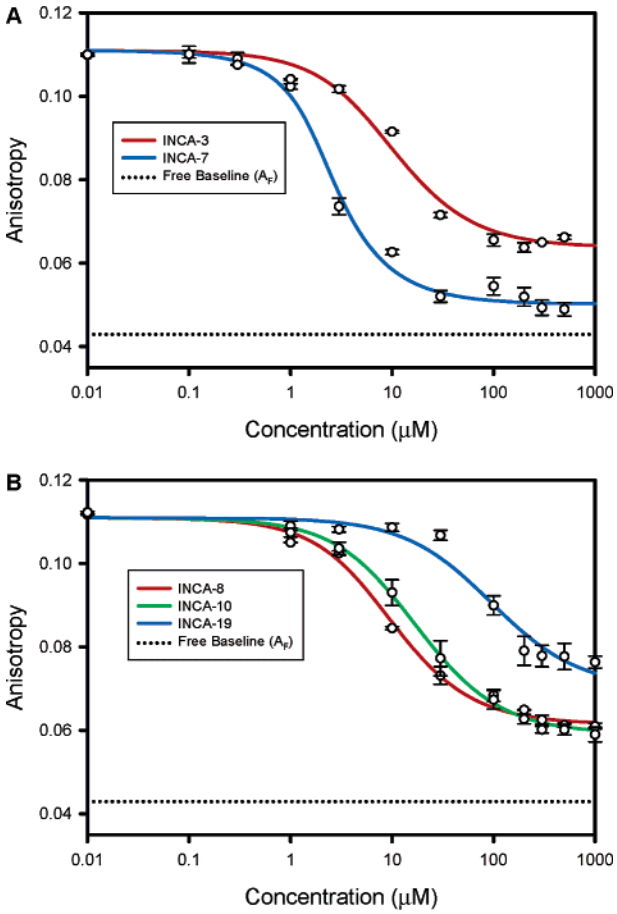

FIGURE 6: Incomplete competitive behavior of certain INCA compounds. This behavior can be explained by an anticooperative four-state model (*21*). (A) INCA-3 and INCA-7 and (B) INCA-8, INCA-10, and INCA-19 are grouped together to minimize data overlap. INCA-5, INCA-9, and INCA-12 exhibit similar curves, but have been omitted for clarity. Note that the compounds do not reduce fluorescence anisotropy to the free OG-VIVIT baseline (dotted lines).

ternary than from binary complexes; i.e., a small-molecule inhibitor will exert an anticooperative modulatory influence. However, complete dissociation of OG-VIVIT will not occur, even in the presence of an increasingly high inhibitor concentration (see eq 28 from ref *21*). These predictions reflect precisely our experimental findings (Figure 6 and Table 4). It can be readily seen that a smaller value of K_{D3} (i.e., closer to $K_{D1} = 0.5$ μM) corresponds to a smaller achievable reduction of anisotropy. This means that some compounds, such as INCA-12, may have an intrinsically high affinity for Cn, but only slightly affect VIVIT binding. Physical interpretations of this scenario could be that the compound and peptide bind to neighboring sites and mutually alter binding site geometry, or that the binding sites are partially overlapping, allowing VIVIT access to only a subset of its normal binding interface.

The finding may be practically significant, since the identification of compounds with neighboring binding epitopes is gaining increasing pharmacologic attention for the design of high-affinity ligands through a linked-fragment strategy (*30*). Our analysis provides an FP approach to such compounds, which would otherwise likely be discarded. One could envision that one or several of the incompletely competing INCAs might be combined to improve binding

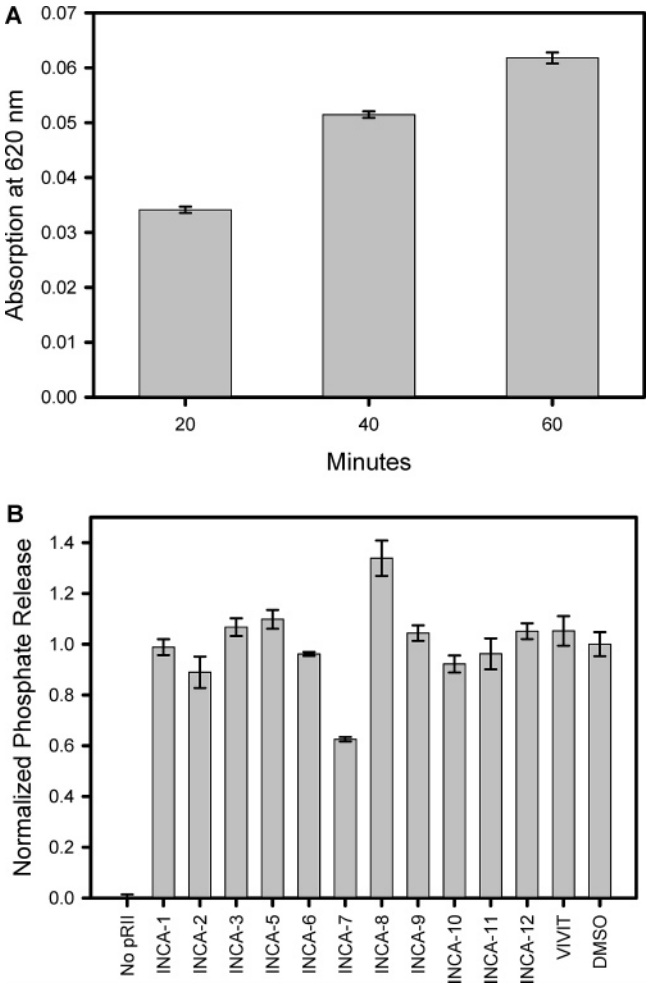

FIGURE 7: (A) Release of phosphate from the pRII peptide in the presence of 5 μM Cn after incubation for the indicated times. In this colorimetric assay, the amount of free phosphate is proportional to the absorption at 620 nm. (B) Release of phosphate from the pRII peptide in the presence of 5 μM Cn and 50 μM INCAs or VIVIT after 30 min. Phosphate release is shown normalized to the 5% (v/v) DMSO control. In the absence of pRII, no free phosphate was detected.

affinity and to enlarge the repertoire of structures for the disruption of the NFAT−Cn interaction.

We next asked whether the identified compounds would affect the enzymatic activity of the catalytic domain of Cn. Since INCAs were identified as competitors to the VIVIT/NFAT site on Cn and since VIVIT does not inhibit dephosphorylation of substrates that do not require this NFAT docking site (*23*), we hypothesized that the compounds would not perturb the intrinsic enzymatic activity of the catalytic domain of Cn. We found that the recombinant catalytic domain of Cn was constitutively active toward the RII phosphopeptide without a requirement for the B subunit or calmodulin (Figure 7A). Furthermore, Cn dephosphorylated the RII phosphopeptide in the presence of excess amounts of INCA compounds (Figure 7B). In fact, the Cn catalytic activity with compounds was very similar to the activity in the presence of no compound (DMSO control) or the VIVIT peptide. We conclude that INCAs interact with Cn in a way that does not significantly compromise the active site. This finding illustrates a concept of substrate-selective enzyme inhibition (SSEI), i.e., targeted inhibition of a specific enzyme−substrate docking site while potentially preserving catalytic activity toward other substrates.

SUMMARY

This paper discusses the optimization of conditions for HTP FP assays and their successful application to the identification of small organic molecules for the targeted inhibition of the NFAT−Cn interaction. Entire protein−protein interactions are often difficult to study in HTP formats. To make the system amenable to HTP FP, we reduced the problem to a peptide−protein interaction. To this end, we introduced the idea to use an NFAT-surrogate peptide corresponding to the primary binding epitope with Cn. We illustrated by experiments and theoretical calculations that a second level of optimization was crucial before embarking on a small-molecule screen, i.e., >55-fold *in vitro* affinity optimization of the wild-type peptide sequence (SPRIEIT) to VIVIT peptide (Figure 3).

We showed that the quantum yield of the OG fluorophore was not dependent on the VIVIT binding state, i.e., whether the peptide was Cn-bound or free (Figure 1A). On the basis of estimated rotational correlation times, we found that experimentally observed anisotropy values were consistent with a specific binding model (Figure 1B). We introduced the concept of a figure of merit, Φ, for selecting optimal FP assay conditions and demonstrated that the chosen fluorophore had a nearly optimal fluorescence lifetime for the OG-VIVIT−Cn assay (Figure 2). We devised a rational approach to the choice of assay conditions based on (i) FP sensitivity analysis (Table 1) and (ii) calculation of assay quality parameters (Table 2). The concentration range of screened compounds could then be chosen so that we could focus on potential hits with dissociation constants of $\leq$100 μM (Figure 4). The successful tuning of assay conditions was demonstrated by the identification of novel small-molecule inhibitors of NFAT−Cn association (INCAs, Figure 5 and Table 3). INCA compounds with both complete and incomplete dissociation capabilities were discovered (Figure 6 and Table 4). Furthermore, we demonstrated that the catalytic activity of Cn *per se* was not diminished in the presence of INCAs (Figure 7). The compounds should be amenable to direct lead optimization and/or synthetic exploration via linked-fragment strategies.

Our further study established that at least one of our compounds, INCA-6, is cell-permeable and efficiently blocks Cn-dependent dephosphorylation of NFAT and induction of NFAT target genes in cultured T cells, but preserves the catalytic activity of Cn *per se* (*20*). In this context, it is, therefore, more selective than the currently established immunosuppressive drugs cyclosporin A and FK506.

MATERIALS AND METHODS

Experiments were carried out essentially as described elsewhere (*20*). In brief, the catalytic domain of human Cn Aα was overexpressed as a GST fusion protein in *Escherichia coli* and purified using affinity and gel filtration columns. Final buffer conditions were 10 mM Tris-HCl (pH 7.4), 50 mM NaCl, and 1 mM $CaCl_2$ without a reducing agent.

The VIVIT peptide was synthesized with the sequence NH_2-GPHPVIVITGPHEE-$CONH_2$, and the SPRIEIT peptide

was prepared as the sequence NH_2-SGPSPRIEITPSH-$CONH_2$ (Tufts University, Boston, MA). The 5-succinimidyl ester of Oregon Green (OG) 488 carboxylic acid (Molecular Probes, Eugene, OR) was used for fluorophore coupling.

Polarized fluorescence intensities were measured at 20 °C on an Analyst instrument (Molecular Devices, Sunnyvale, CA) with excitation and observed emission wavelengths of 485 and 530 nm, respectively. Fluorescence measurements from the two perpendicular detectors were each corrected for background counts based on a buffer standard without a fluorophore. *G* factor correction was performed using a fluorescein standard.

High-throughput compound screening was carried out with 0.5 μM Cn, 30 nM OG-VIVIT, and 40 nL of compound (5 mg/mL in DMSO). Compounds were obtained from ChemBridge (San Diego, CA), AsInEx, and Maybridge. The fluorescence intensity of a sample was expressed as $I^{=} + 2I^{\perp}$, where $I^{=}$ and $I^{\perp}$ are intensities parallel and perpendicular to the plane of polarized incident light, respectively. Levenberg−Marquardt nonlinear least-squares fitting of the complete competitive binding model described by eqs 17 and 39 from ref *21* was accomplished with SigmaPlot 2001 (SPSS, Chicago, IL). Fitting of the incomplete competitive binding model described by eqs 27 and 39 from ref *21* was accomplished with MLAB (Civilized Software, Silver Spring, MD), which allows nonlinear least-squares fitting of implicitly defined functions. Parameter estimates are given ± the standard error of the mean, and fluorescence intensity distributions are given as means ± one standard deviation.

Dephosphorylation of 0.15 mM pRII peptide (Biomol, Plymouth Meeting, PA) by the catalytic domain of Cn was assessed at 25 °C in 50 mM Tris-HCl (pH 7.4), 100 mM NaCl, 6 mM $MgCl_2$, 0.5 mM $CaCl_2$, 0.025% (v/v) NP-40, and 5% (v/v) DMSO, but without a reducing agent. The presence of 0% up to at least 10% (v/v) DMSO had no detectable influence on Cn activity. At given time points, 50 μL dephosphorylation reactions were terminated by addition of 100 μL of Biomol Green reagent, and the release of free phosphate was monitored photometrically at 620 nm after color had developed for 20 min. Freshly distilled H_2O was used. No free phosphate could be detected when either no Cn or heat-denatured Cn was added.

APPENDIX

1. Estimation of Rotational Correlation Times. The rotational correlation time of nonspherical particles can be estimated on the basis of results by J. B. Perrin for prolate and oblate ellipsoids (*31*). In the following, we denote with *a* the long and *b* the short semiaxis of the ellipsoid. f_a, f_b, and f_{Sph} are the observed frictional coefficients for rotation about *a*, for rotation about *b*, and of a sphere of equivalent volume, respectively. The frictional coefficient ratios can be expressed as eqs A1 and A2.

$$\frac{f_a}{f_{Sph}} = \frac{4(1-p^2)}{3(2-p^2S)} \tag{A1}$$

$$\frac{f_b}{f_{Sph}} = \frac{4(1-p^4)}{3p^2[S(2-p^2)-2]} \tag{A2}$$

Equations A3 and A4 define *S* and *p* for the case of a prolate ellipsoid, by which we will approximate the rotational shape of OG-VIVIT.

$$S = \frac{2\ln\left(\frac{1+\sqrt{1-p^2}}{p}\right)}{\sqrt{1-p^2}} \tag{A3}$$

$$p = \frac{b}{a} \tag{A4}$$

It can be seen that only an estimate of the ratio of the semiaxes is required, but not knowledge about their absolute lengths. The rotational behavior of prolate ellipsoids is further characterized by eqs A5 and A6, where τ_a, τ_b, and τ_{Sph} denote the rotational correlation times about *a*, about *b*, and for the equivalent sphere, respectively.

$$\tau_a = \frac{f_b}{f_{Sph}}\tau_{Sph} \tag{A5}$$

$$\tau_b = 2\left(\frac{f_{Sph}}{f_a} + \frac{f_{Sph}}{f_b}\right)^{-1} \times \tau_{Sph} \tag{A6}$$

The overall correlation time, τ_C, is described by eq A7.

$$\tau_C = \frac{3}{\tau_a^{-1} + 2\tau_b^{-1}} \tag{A7}$$

Using this formalism, we attempted to estimate *p* for OG-VIVIT. Assuming a roughly α-helical geometry (14 amino acid residues, neglecting the fluorophore), we estimated $2a \approx 14 \times 1.5$ Å $= 21$ Å and $2b \approx 6$ Å, corresponding to a value of *p* on the order of $^2/_7$. Starting from a τ_{Sph} of 0.8 ns, we concluded that $\tau_{CF} = 1.1$ ns. It should be emphasized that the preceding calculation is a very rough estimate, designed to provide an approximation for the sole purpose of analyzing whether the observed anisotropy data could be explained by purely specific binding behavior, or whether significant nonspecific binding could have occurred (*21*).

2. Optimal Choice of a Fluorophore Lifetime. On the basis of eq 1, we define the figure of merit, Φ, as a function of τ_F according to eq A8 (Figure 2).

$$\Phi(\tau_F) = \left(1 + \frac{\tau_F}{\tau_{CB}}\right)^{-1} - \left(1 + \frac{\tau_F}{\tau_{CF}}\right)^{-1} \tag{A8}$$

where $\tau_{CB} > \tau_{CF}$.

The physically meaningful global maximum of Φ is obtained for τ_F^{OPT} as given by eq A9.

$$\tau_F^{OPT} = \sqrt{\tau_{CB}\tau_{CF}} \tag{A9}$$

The optimum corresponds to the geometric mean of bound and free rotational correlation times. In our particular case, we found that $\tau_{CB} = 16.3$ ns, $\tau_{CF} = 1.1$ ns, and hence $\tau_F^{OPT} = 4.3$ ns, which is very close to the OG lifetime of ∼4 ns.

NOTE ADDED AFTER ASAP PUBLICATION

This paper was published prematurely 11/26/04. An author has been removed from ref *21*. The correct version of the paper was published 11/30/04.

REFERENCES

1. Peczuh, M. W., and Hamilton, A. D. (2000) Peptide and protein recognition by designed molecules, *Chem. Rev. 100*, 2479−2494.

2. Cochran, A. G. (2000) Antagonists of protein−protein interactions, *Chem. Biol. 7*, R85−R94.
3. Toogood, P. L. (2002) Inhibition of protein−protein association by small molecules: Approaches and progress, *J. Med. Chem. 45*, 1543−1558.
4. Strausberg, R. L., and Schreiber, S. L. (2003) From knowing to controlling: A path from genomics to drugs using small molecule probes, *Science 300*, 294−295.
5. Jones, S., and Thornton, J. M. (1996) Principles of protein−protein interactions, *Proc. Natl. Acad. Sci. U.S.A. 93*, 13−20.
6. Lo Conte, L., Chothia, C., and Janin, J. (1999) The atomic structure of protein−protein recognition sites, *J. Mol. Biol. 285*, 2177−2198.
7. Aramburu, J., Rao, A., and Klee, C. B. (2000) Calcineurin: From structure to function, *Curr. Top. Cell. Regul. 36*, 237−295.
8. Crabtree, G. R., and Olson, E. N. (2002) NFAT signaling: Choreographing the social lives of cells, *Cell 109* (Suppl.), S67−S79.
9. Hemenway, C. S., and Heitman, J. (1999) Calcineurin. Structure, function, and inhibition, *Cell. Biochem. Biophys. 30*, 115−151.
10. Horsley, V., and Pavlath, G. K. (2002) NFAT: Ubiquitous regulator of cell differentiation and adaptation, *J. Cell Biol. 156*, 771−774.
11. Masuda, E. S., Imamura, R., Amasaki, Y., Arai, K., and Arai, N. (1998) Signalling into the T-cell nucleus: NFAT regulation, *Cell. Signalling 10*, 599−611.
12. Rao, A., Luo, C., and Hogan, P. G. (1997) Transcription factors of the NFAT family: Regulation and function, *Annu. Rev. Immunol. 15*, 707−747.
13. Rusnak, F., and Mertz, P. (2000) Calcineurin: Form and function, *Physiol. Rev. 80*, 1483−1521.
14. Shibasaki, F., Hallin, U., and Uchino, H. (2002) Calcineurin as a multifunctional regulator, *J. Biochem. 131*, 1−15.
15. van Rooij, E., Doevendans, P. A., de Theije, C. C., Babiker, F. A., Molkentin, J. D., and de Windt, L. J. (2002) Requirement of nuclear factor of activated T-cells in calcineurin-mediated cardiomyocyte hypertrophy, *J. Biol. Chem. 277*, 48617−48626.
16. Wilkins, B. J., De Windt, L. J., Bueno, O. F., Braz, J. C., Glascock, B. J., Kimball, T. F., and Molkentin, J. D. (2002) Targeted disruption of NFATc3, but not NFATc4, reveals an intrinsic defect in calcineurin-mediated cardiac hypertrophic growth, *Mol. Cell. Biol. 22*, 7603−7613.
17. Takayanagi, H., Kim, S., Koga, T., Nishina, H., Isshiki, M., Yoshida, H., Saiura, A., Isobe, M., Yokochi, T., Inoue, J., Wagner, E. F., Mak, T. W., Kodama, T., and Taniguchi, T. (2002) Induction and activation of the transcription factor NFATc1 (NFAT2) integrate RANKL signaling in terminal differentiation of osteoclasts, *Dev. Cell 3*, 889−901.
18. Molkentin, J. D., Lu, J. R., Antos, C. L., Markham, B., Richardson, J., Robbins, J., Grant, S. R., and Olson, E. N. (1998) A calcineurin-dependent transcriptional pathway for cardiac hypertrophy, *Cell 93*, 215−228.
19. Kiani, A., Rao, A., and Aramburu, J. (2000) Manipulating immune responses with immunosuppressive agents that target NFAT, *Immunity 12*, 359−372.
20. Roehrl, M. H. A., Kang, S., Aramburu, J., Wagner, G., Rao, A., and Hogan, P. G. (2004) Selective inhibition of calcineurin-NFAT signaling by blocking protein−protein interaction with small organic molecules, *Proc. Natl. Acad. Sci. U.S.A. 101*, 7554−7559.
21. Roehrl, M. H. A., Wang, J. Y., and Wagner, G. (2004) A general framework for development and data analysis of competitive high-throughput screens for small-molecule inhibitors of protein−protein interactions by fluorescence polarization, *Biochemistry 43*, 16056−16066.
22. Aramburu, J., Garcia-Cozar, F., Raghavan, A., Okamura, H., Rao, A., and Hogan, P. G. (1998) Selective inhibition of NFAT activation by a peptide spanning the calcineurin targeting site of NFAT, *Mol. Cell 1*, 627−637.
23. Aramburu, J., Yaffe, M. B., Lopez-Rodriguez, C., Cantley, L. C., Hogan, P. G., and Rao, A. (1999) Affinity-driven peptide selection of an NFAT inhibitor more selective than cyclosporin A, *Science 285*, 2129−2133.
24. Rosner, B. (1995) *Fundamentals of Biostatistics*, 4th ed., Wadsworth, Belmont.
25. Tetin, S. Y., and Hazlett, T. L. (2000) Optical spectroscopy in studies of antibody-hapten interactions, *Methods 20*, 341−361.
26. Jameson, D. M., and Seifried, S. E. (1999) Quantification of protein−protein interactions using fluorescence polarization, *Methods 19*, 222−233.
27. Garcia De La Torre, J., Huertas, M. L., and Carrasco, B. (2000) Calculation of hydrodynamic properties of globular proteins from their atomic-level structure, *Biophys. J. 78*, 719−730.
28. Zhang, J. H., Chung, T. D., and Oldenburg, K. R. (1999) A simple statistical parameter for use in evaluation and validation of high throughput screening assays, *J. Biomol. Screening 4*, 67−73.
29. Lipinski, C. A., Lombardo, F., Dominy, B. W., and Feeney, P. J. (1997) Experimental and computational approaches to estimate solubility and permeability in drug discovery and development settings, *Adv. Drug Delivery Rev. 23*, 3−25.
30. Szczepankiewicz, B. G., Liu, G., Hajduk, P. J., Abad-Zapatero, C., Pei, Z., Xin, Z., Lubben, T. H., Trevillyan, J. M., Stashko, M. A., Ballaron, S. J., Liang, H., Huang, F., Hutchins, C. W., Fesik, S. W., and Jirousek, M. R. (2003) Discovery of a potent, selective protein tyrosine phosphatase 1B inhibitor using a linked-fragment strategy, *J. Am. Chem. Soc. 125*, 4087−4096.
31. Cantor, C. R., and Schimmel, P. R. (1980) in *Biophysical Chemistry*, pp 562−565, Freeman, New York.

BI048232O